Geochimica et Cosmochimica Acta 422 (2026) 385–396

Contents lists available at ScienceDirect

Geochimica et Cosmochimica Acta

journal homepage: www.elsevier.com/locate/gca

A Mesozoic high-elevation plateau in eastern North China? Evidence from detrital zircons☆

Ziyi Guo [a,*], Ming Tang [a], Hehe Jiang [b], Xuyang Zheng [a]

[a] SKLab-DeepMinE, MOEKLab-OBCE, School of Earth and Space Sciences, Peking University, China
[b] State Key Laboratory of Lithospheric and Environmental Coevolution, Institute of Geology and Geophysics, Chinese Academy of Sciences, Beijing, China

ARTICLE INFO

Executive Guest Editor: Fang-Zhen Teng

Keywords:
Eastern North China Plateau
Eu anomaly
Detrital zircon
Crustal thickness

ABSTRACT

High-elevation plateaus form as the culmination of tectonic and magmatic processes, and they influence surface processes such as erosion and sedimentation. There are signs indicating high topographies in eastern North China (ENC) during the Mesozoic, coinciding with the reactivation and dramatic destruction of the North China Craton. However, the topographic evolution of ENC and how this evolution may be related to the North China Craton destruction are unclear. To constrain the topographic evolution in ENC, we measured Eu anomalies (a proxy for crustal thickness) in ~5000 detrital zircons from modern river sands and ancient sandstones to reconstruct the crustal thickness evolution of ENC in the Mesozoic. Our results show that the ENC crust thickened to ~60–70 km, similar to that of Tibet, from the early-middle Jurassic through the early Cretaceous, followed by a gradual thinning process during the late Cretaceous. Our crustal thickness results are consistent with whole-rock La/Yb results and geologic records that are indicative of crustal contraction and extension. We further note that a similar thickening trend is seen in multiple regions within ENC, which leads us to propose the existence of a vast Mesozoic plateau in ENC. Additionally, we find that the proportion of Mesozoic zircons in sandstones gradually increases with depositional age, reaching a peak in the Late Cretaceous, and then decreases rapidly in younger samples. This pattern likely reflects changes in erosion rates controlled by evolving topography, and thus records the growth and collapse of a plateau. Notably, the peak in Mesozoic detrital zircon proportion occurs approximately 50 Myr after the maximum uplift period of the ENC plateau, suggesting a time lag between uplift and sedimentary response. Based on our results, we model the erosion processes of the plateau and find that this time lag can be readily explained by the uplifting history reconstructed from our detrital zircon Eu anomaly data if the climate was largely arid. The intense thickening of the ENC crust was likely driven by the low-angle subduction of the Izanagi plate, with additional contributions from surrounding circum-craton orogenies. At ~130 Ma, the rollback of the Izanagi plate likely resulted in both the collapse of the plateau and the destruction of the North China Craton.

1. Introduction

The North China Craton experienced remarkable reactivation during the Mesozoic era, characterized by extensive and intense geological activities across the craton that had remained stable for over a billion years (Kusky et al., 2007b; Dong et al., 2015; Wang et al., 2018a; Wu et al., 2019). This time period witnessed a transition from a compressional regime in the Jurassic to an extensional regime in the Cretaceous, accompanied by fundamental changes in magmatic activity, including a shift in migration direction and an increase in magmatic intensity. Specifically, U-Pb age data show that Jurassic magmatism in the NCC exhibits a westward younging trend, whereas Early Cretaceous magmatism displays an eastward younging trend (Wu et al., 2019; Ma and Xu, 2021). These tectono-magmatic processes are generally believed to be related to the subduction of the Izanagi plate (a major plate in the Paleo-Pacific tectonic system) (Wu et al., 2019; Zhu and Xu, 2019; Liu et al., 2024). Intense tectono-magmatic processes eventually culminated in the massive destruction of the North China Craton during the Early Cretaceous (Dong et al., 2015; Wu et al., 2019). As a result of this catastrophic event, the thick lithospheric mantle beneath the eastern

☆ This article is part of a special issue entitled: 'In honor of Bill McDonough' published in Geochimica et Cosmochimica Acta.

* Corresponding author.
E-mail address: guoziyi@stu.pku.edu.cn (Z. Guo).

https://doi.org/10.1016/j.gca.2025.06.019
Received 18 February 2025; Accepted 22 June 2025
Available online 23 June 2025
0016-7037/© 2025 Elsevier Ltd. All rights are reserved, including those for text and data mining, AI training, and similar technologies.

North China Craton was largely removed and replaced by a juvenile lithospheric mantle (Kusky et al., 2007a; Liu et al., 2019; Wu et al., 2019).

Prior to the peak destruction of the North China Craton, intense *syn*-orogenic crustal shortening, thickening, and metamorphism likely occurred, resulting in prolonged compression in the North China Craton (Dong et al., 2015; Liu et al., 2019). Contractional structures, such as large-scale thrust faults and folds, were particularly abundant in the eastern block of the North China Craton, encompassing northern Hebei, western Shandong, and Liaoning provinces (Davis et al., 2001; Wu et al., 2007; Li et al., 2012; Dong et al., 2015). Prolonged compression, in turn, may have led to intense crustal thickening and uplift.

Previous studies have reported signs of high elevations in eastern North China (ENC) during the Mesozoic. For example, granitic rocks with high La/Yb and Sr/Y ratios were found in the Liaodong-Shandong Peninsula, which were proposed to have formed by mixing of thickened ancient lower crust and magmas derived from lithospheric mantle (Zhang et al., 2009; Zhang and Jiao, 2020; Liang et al., 2020; Liu et al., 2023). Paleo-elevations estimated from basalt vesicularity and clumped isotope palaeothermometry may have reached >4 km in the northeastern China during the Early Cretaceous (Xia et al., 2012; Zhang et al., 2021b). Furthermore, the expansion and migration of the Jehol Biota, a remarkable terrestrial lagerstätte known for preserving exquisite large fossils, may also reflect the influence of climate change driven by regional elevation changes (Pan et al., 2013; Zhou et al., 2021). More recently, Wang et al. (2024) identified systematic spatiotemporal variations in skarn garnet oxygen isotopes in eastern China and interpreted these variations as a consequence of the existence of an eastern coastal plateau in the Jurassic.

While the previous studies are indicative of high topographies in the Mesozoic ENC, its uplifting history and spatial extent remain uncertain. In addition, the coupling between this topographic evolution and tectonic transition as well as the destruction of the North China Craton is poorly understood. To address these questions, we carried out extensive sampling of modern river sands and sandstones deposited since the early Jurassic. We focused on analyzing Eu anomalies ($Eu/Eu^*=Eu_n/\sqrt{(Sm_n \times Gd_n)}$, where subscript n denotes a chondrite normalized concentration) and U-Pb age distributions of detrital zircons separated from these samples. These data allow us to calculate the crustal thickness evolution in ENC. We then place our results on crustal thickness and age distributions in an erosion model to understand the erosion history of ENC. These results together provide new insights into the fate of ENC during the Mesozoic craton destruction and tectonic transition.

2. Geological background and samples

The North China Craton can be divided into the eastern and western blocks by Trans-North China Orogeny (Zhao et al., 2000, 2001). These two blocks amalgamated into a stable craton through arc/continent collision. They initially sutured at ~2.5 Ga, followed by multiple episodes of arc accretion and orogenic reworking until ~1.8 Ga (Kusky et al., 2016; Zhu et al., 2021). Along the northern margin, the newly assembled Siberia and North China blocks collided during 1.90–1.85 Ga, as supported by the palaeomagnetic and orogenic records (Kusky and Li, 2003; Kusky et al., 2016; Li et al., 2023). The basement of the North China Craton is mainly Archean to Paleoproterozoic (Zhang et al., 2023; Diwu et al., 2024). Detrital zircon U-Pb ages show two main peaks of ~1.85 Ga and ~2.5 Ga, which are probably related to the orogenic and

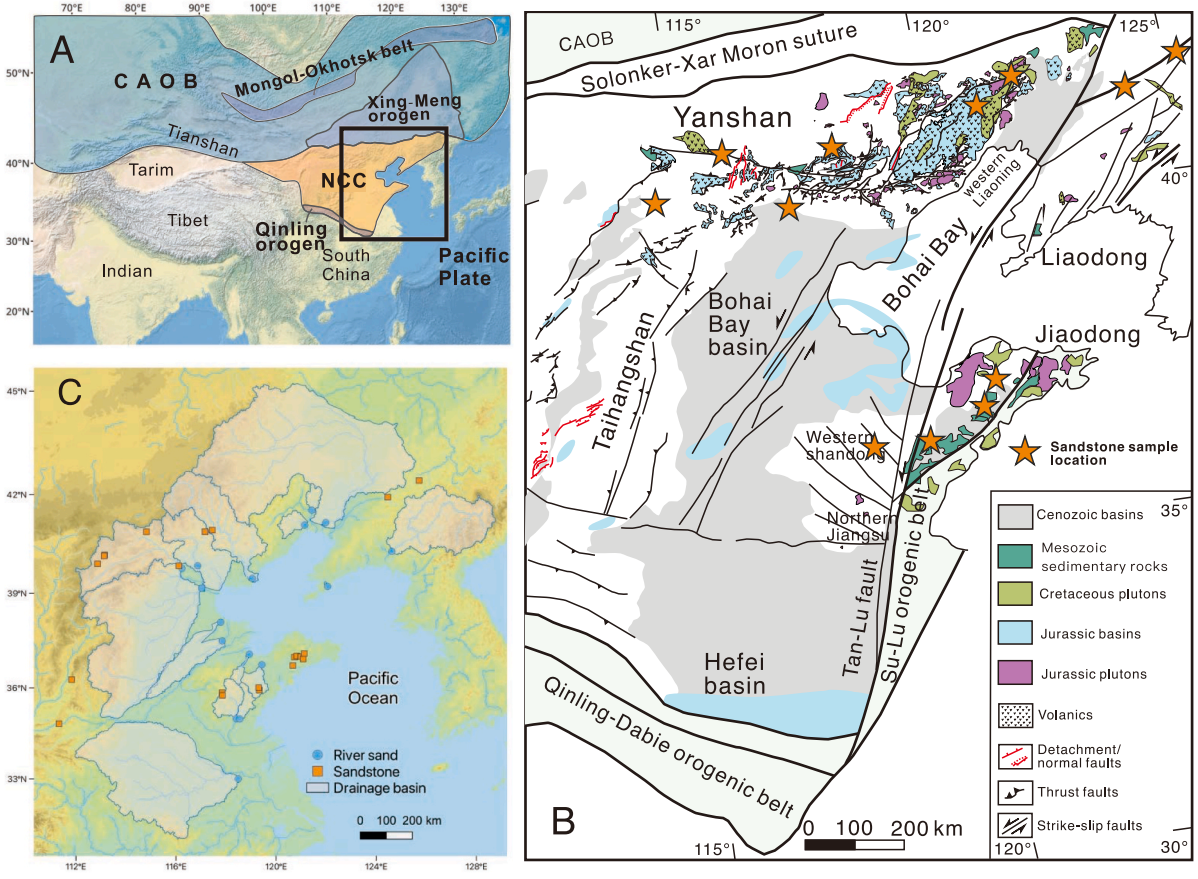


Fig. 1. Maps showing the geological background of ENC and sampling sites. (A) Tectonic map showing the location of NCC and its eastern part (black window). CAOB: Central Asia Orogenic Belt. (B) Simplified geological map of NCC showing the Jurassic-Cretaceous rocks and structures (Modified from Qiu et al., 2023). (C) Sample sites and drainage basin of rivers.

metamorphic events associated with continental amalgamation (Zhao and Zhai, 2013; Zhang et al., 2023; Diwu et al., 2024).

Since its formation, the North China Craton had remained stable until the massive circum-craton subduction and collisional orogenies (Kusky et al., 2007b; Dong et al., 2015; Liu et al., 2019) (Fig. 1B). To the north of ENC lies Xing-Meng orogeny, which is the southern part of the Central Asian Orogenic Belt formed by the closure of Paleo-Asian Ocean until the Triassic (Xu et al., 2013; Xiao et al., 2015; Wan et al., 2018). Farther north, the Mongol-Okhotsk orogenic belt resulted from the west-to-east diachronous closure of the Mongol-Okhotsk Ocean. This closure led to the amalgamation of the Siberian and North China-Mongolian blocks along the Mongol-Okhotsk suture during the Early to Middle Mesozoic (Van Der Voo et al., 2015; Sorokin et al., 2020; Zhao et al., 2024). To the south, following the collision between the South and North China blocks, the Qinling orogeny was formed during the late Permian to Triassic period (Wu and Zheng, 2013; Zhao et al., 2023). The initial westward subduction of Izanagi plate began as early as the early Jurassic as evidenced by magmatic migration (Kusky et al., 2014; Zhu and Xu, 2019), which may have reactivated the craton margin (Liu et al., 2019).

Eastern North China (roughly corresponding to the eastern block of the North China Craton) is surrounded by the Central Asian Orogenic Belt to the north, Qinling orogeny to the south, and Taihang Mountains to the west, and it extends to the western part of Korea (Fig. 1B). We collected modern river sands and sandstones across ENC (Fig. 1C) and divided them into four subregions: Shandong, Hebei, Liaoning and Shanxi.

Our river sand sampling strategies are based on hydrological analysis. Specifically, we sampled the river sands from downstream sections to maximize coverage of the upstream drainage areas of Mesozoic rocks. The drainage basin of each river is shown in Fig. 1C. The depositional ages of sandstones span from the Jurassic to the early Paleogene. Most of the sandstones were deposited during the early Cretaceous, especially in Shandong province. The Jurassic sandstones younger than 180 Ma are exposed mainly in northern Shanxi, Liaoning and northern Hebei. We analyzed 4879 detrital zircons from 22 sandstone and 15 river sand samples in total. Detailed information is given in the **Supplementary Material 1**.

3. Methods

3.1. Analytical Methods

Detrital zircons separated from the river sands and sandstones were analyzed at Beijing Quick-Thermo Science & Technology Co., Ltd. and Beijing Zhongkekuangyan Test Technology Co., Ltd. Both labs used an ESI New Wave NWR 193^{UC} (TwoVol2) laser ablation system connected to an Agilent 8900 ICP–QQQ. Individual zircon grains were ablated in a constant stream of He carrier gas entering the ICP. Before each analytical session, we optimized the laser and ICP settings for high sensitivities while maintaining $^{232}Th^{16}O^{+}/^{232}Th^{+} \leq 0.2$ %.

The analyses were conducted with a 32 μm spot size, ~4 J/cm^2 laser fluence, and a 5 Hz repetition rate. Each analysis comprises 10 s of background signal collection followed by 20 s of zircon data collection. We used zircon 91500 as the external standard and zircon SA01 as the monitor standard for U-Pb dating. For trace elements, NIST 610 glass was used as the external reference material and Si as the internal standard. Zircon 91500 and NIST 610 were measured twice, both before and after 8–10 sample analyses. Repeated analyses of zircon SA01 yielded a mean $^{206}Pb/^{238}U$ age of 534.23 ± 0.77 Ma and a Eu/Eu* of 1.12 ± 0.15 (2 SD) (Fig. S1 and S2), consistent with the recommended values (Huang et al., 2019).

3.2. Crustal thickness and elevation reconstruction

We employed the zircon Eu anomaly proxy to constrain the average crustal thickness over time in ENC. The empirical relationship between crustal thickness and Eu anomaly in zircon was calibrated by Tang et al. (2021):

$$H = (84.2 \pm 9.2) \times Eu/Eu^{*}_{zircon} + (24.5 \pm 3.3) \quad (1)$$

This method is based on the pressure-dependent stability of plagioclase and garnet: plagioclase crystallization at low pressure depletes Eu^{2+}, lowering zircon Eu/Eu*, while garnet stabilization at high pressure oxidizes Eu and enhances bulk Eu partitioning in zircon, increasing zircon Eu/Eu* (Tang et al., 2021). This approach has been successfully applied to reconstruct crustal thickness evolution in the Gangdese Belt in southern Tibet and the Sierra Nevada Batholith in western USA (Tang et al., 2021, 2024b).

Recent studies employing phase equilibria and geochemical modeling have demonstrated that factors such as oxygen fugacity and water content significantly influence the Eu anomaly in zircon (Yakymchuk et al., 2023; Roberts et al., 2024). These factors may complicate the empirical relationship used for estimating crustal thickness, thereby raising concerns about the reliability of the Eu/Eu* ratio as a valid indicator of crustal thickness (Yakymchuk et al., 2023; Roberts et al., 2024). Taking these concerns into account, Tang et al. (2024b) revisited the Eu anomaly proxy through a case study on the Sierra Nevada batholith. Their findings, consistent with other geological observations relevant to crustal thickening/thinning in the area, suggest that magma redox conditions and water content, may themselves be governed by differentiation pressure and, consequently, crustal thickness. They thus concluded that, with sufficient data and careful processing and interpretation, zircon Eu/Eu* remains a reliable proxy for crustal thickness reconstruction.

We followed the data filtering procedures recommended by Tang et al. (2024b). These filtering procedures excluded data compromised by mineral inclusions, metamorphism, titanite co-crystallization, and those zircons of S-type granite origins. After filtering, 3865 zircon data points remained, of which approximately 35% are of Mesozoic ages. The results are provided in **Supplementary Material 2**.

Over large areas and timescales, elevation is related to crustal thickness following the Airy isostatic compensation model (Airy, 1855). Thus, the elevation h, to first order, can be calculated as:

$$h = (H\text{-}H_0)\left(1\text{-}\frac{\rho_c}{\rho_m}\right) \quad (2)$$

where ρ_c and ρ_m are the densities of the average mantle and continental crust, respectively, and H_0 represents the reference crustal thickness, corresponding to a sea level elevation (Turcotte and Schubert, 2014). Here, we adopted values of $\rho_c = 2.74$ g/cm^3, $\rho_m = 3.24$ g/cm^3, and $H_0 =$ 33 km in ENC, as constrained by geophysical studies (Wei et al., 2015; Xia et al., 2017, 2020).

4. Results

Europium anomalies in detrital zircons suggest that ENC experienced significant changes in calculated crustal thickness (Fig. 2). In the Late Triassic, the crustal thickness was 40–50 km. Throughout the Early to Late Jurassic, the crust progressively thickened, reaching up to 70 km at ~170 Ma, and then remained stable until ~120 Ma. This strongly thickened crust persisted for about 50 million years before thinning to 30–35 km, consistent with its present-day thickness (Chen, 2009). Our reconstructed crustal thickness evolution of ENC is broadly consistent with that calculated from whole-rock La/Yb_n ratios (Fig. 2C). However, due to the paucity of whole-rock data, the crustal thickness estimates are less well constrained than those derived from detrital zircons. Based on the changes in crustal thickness, we divided the evolution of ENC into three stages: contractional stage (~200 to ~140 Ma), transitional stage (~140 to ~110 Ma), and extensional stage (~110 to ~80 Ma).

We also divided our data into four subsets, classifying sandstone

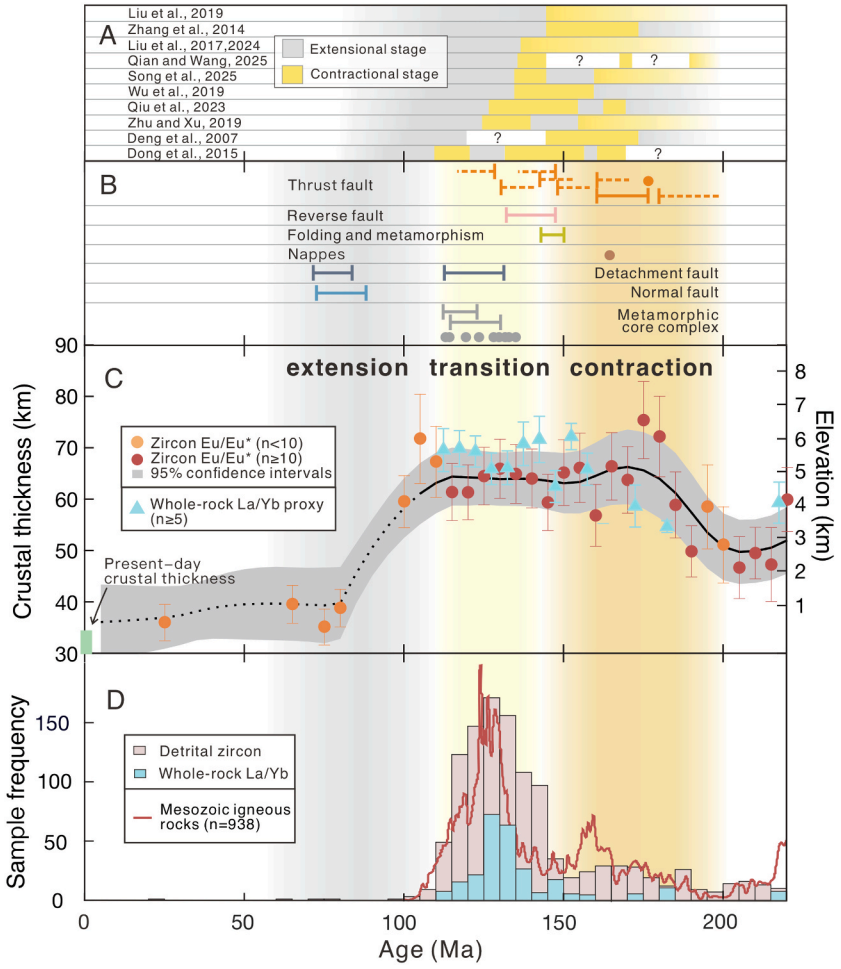


Fig. 2. Reconstructed crustal thickness evolution of ENC based on detrital zircons and whole-rock La/Yb_n data. (A) Compilation of tectonic regime subdivisions of the NCC. (B) Timeline of geological events (after Wang et al., 1990; Davis et al., 2001; Lin et al., 2011b; Zhang et al., 2014a; Zhu et al., 2015; Dong et al., 2015; Zeng et al., 2022; Qiu et al., 2023; Song et al., 2025; Qian and Wang, 2025). Contractional structures include thrust, folds, and nappes; extensional structures include normal faults, detachment faults and metamorphic core complex. Dashed lines indicate the upper or lower age boundaries of these events. (C) Calculated crustal thickness of ENC using Eu anomaly of detrital zircons and whole-rock La/Yb_n. Data are plotted as binned averages (bin size = 5 Myr) and 2 standard errors. The black line is the fitting curve of detrital zircon-based calculation. The dashed line indicates intervals with insufficient data. (D) Age distribution of zircons and whole-rock samples from ENC; the intensity of Mesozoic magmatic activity is modified from Zhang et al. (2014a). The three colored bands correspond to the contractional, transitional, and extensional stages. Data sources for whole-rock La/Yb_n are provided in Supplementary Material 2, Dataset 3.

samples based on the provinces where they were collected, and modern river sands based on drainage basins, with subregion names reflecting the main provinces each basin covers. These subsets show largely consistent patterns of crustal thickness evolution. In particular, all four regions are marked by a thickening trend during the late Triassic to early Jurassic (Fig. 3).

In addition to the 22 sandstone samples analyzed in this study, we also compiled detrital zircon age data from 22 additional samples reported in previous studies. The sandstone data show that the proportion of zircons of Mesozoic (and younger) ages first gradually increases with depositional ages from the early-middle Jurassic to the late Cretaceous, reaching up to ~70%, and then decreases rapidly in younger samples (Fig. 4). The proportion of zircons of Mesozoic and younger ages is also low (<30%) in modern river sands.

5. Discussion

We suggest that the Mesozoic zircons from our samples predominantly come from ENC rather than the adjacent orogenic belts formed by other tectonic events. This is because magmatism in the adjacent orogenic belts had generally ceased prior to ~200 Ma, with only a few areas near ENC or the subduction zones experiencing renewed magmatic activities. For example, the majority of granitoids in the Qinling orogeny were formed primarily before 200 Ma (Sun et al., 2002; Wang et al., 2009; Qin et al., 2009). In the Mongol-Okhotsk orogen, most magmatism took place in the Permian (Sorokin et al., 2020; Wang et al., 2022a; Zhao et al., 2024). Although sporadic magmatic activity resumed during the Jurassic to Cretaceous in some of these more ancient orogenies, they are volumetrically minor compared with the magmatic activities in the ENC interior based on their current distributions (Dong et al., 2011). The Xing-Meng orogeny was formed by the closure of the Paleo-Asian Ocean during the late Paleozoic with various magmatic episodes before 200 Ma (Xu et al., 2013; Ouyang et al., 2015; Chen et al., 2023b). The northeastern part of the Xing-Meng orogeny underwent a regional magmatic flare-up during the Early Cretaceous, likely driven by the subduction of the Izanagi plate to the east and the Mongol-Okhotsk ocean to the north (Zhang et al., 2022). These magmatic activities were coeval to those within the ENC plateau. However, based on the Hf isotopic data of detrital zircons within ENC, contributions from this localized magmatism are limited, and the majority of detrital zircons in the ENC area originate from its interior. Only a small number of zircons older than 170 Ma showing positive εHf(t) values may come from the Xing-Meng orogeny (Yang et al., 2006; Liu et al., 2019). Therefore, our reconstructed crustal thickness based on detrital zircons of Mesozoic ages

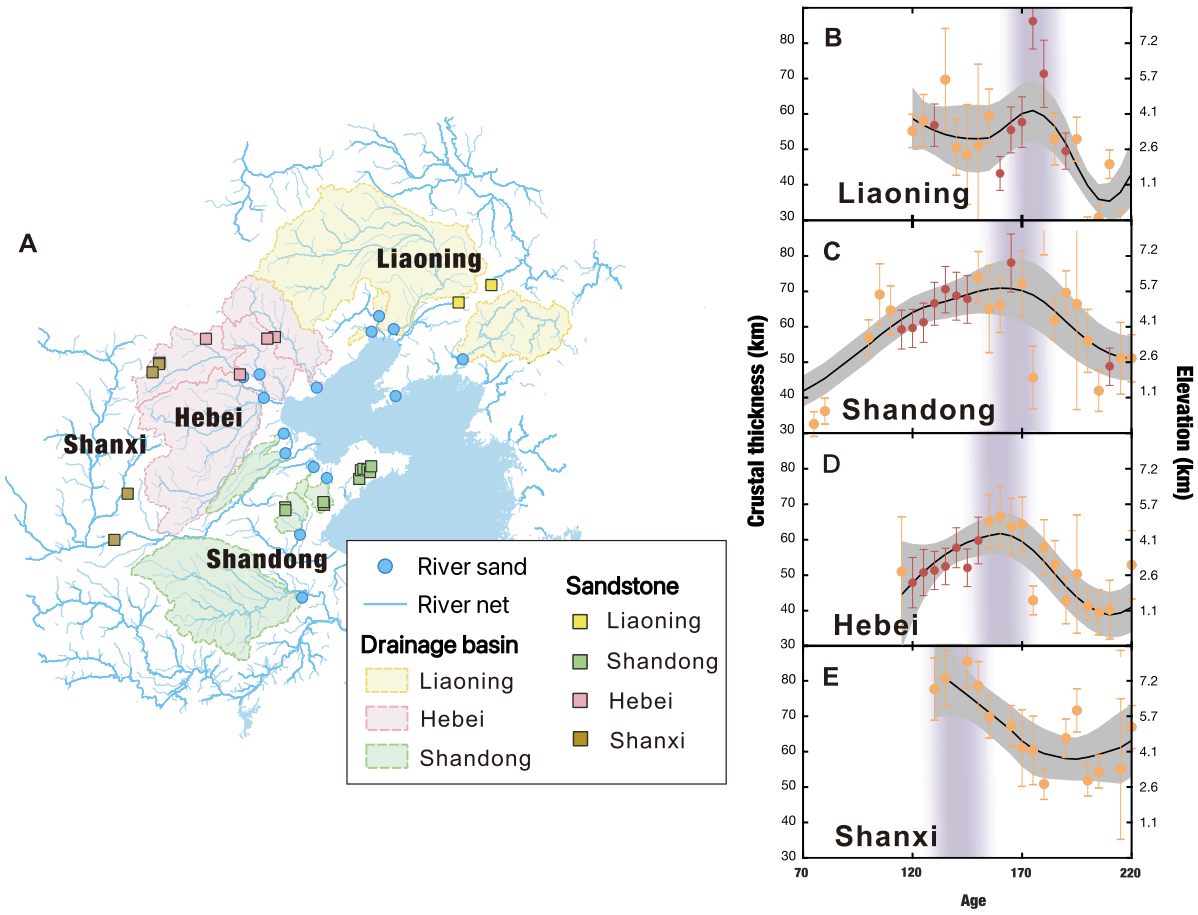


Fig. 3. Crustal thickness reconstruction of four ENC subregions using the same calculation method. (A) Colored regions show drainage basins of the four subregions. The Shanxi subregion includes only sandstone samples. Blue circles represent the sampling locations of river sands, and squares indicate the locations of sandstone samples. (B, C, D, E) Reconstructed crustal thickness histories for the Liaoning, Shandong, Hebei, and Shanxi subregions, respectively. The purple band represents the peak thickness. Other symbols are consistent with those in Fig. 2.

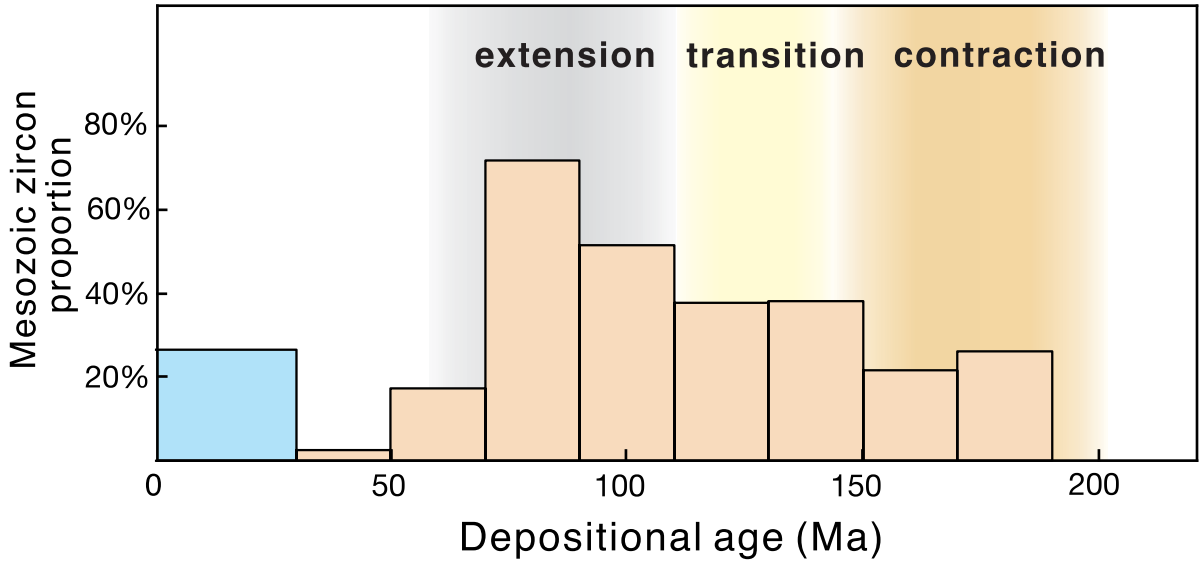


Fig. 4. Mesozoic zircons proportion across different depositional ages (bin size = 20 Myr). The blue bar represents the river sands. The data sources for sandstone depositional ages and detrital zircon ages are provided in Supplementary Material 2.

primarily reflects that of the ENC itself, with minimal influence from the surrounding orogenic belts.

5.1. Crustal thickness evolution of ENC

Our reconstruction results show that the ENC crust began to thicken in the early Jurassic, reaching 60–70 km by 170 Ma (Fig. 2). This crustal thickening process may have resulted from multiple phases of orogenesis in ENC during the Mesozoic, also known as the Yanshanian orogeny (Maruyama et al., 1997; Isozaki et al., 2010; Dong et al., 2015; Zhou and Li, 2017). Initially, the Yanshanian orogeny was divided into two phases (Phase A and Phase B) based on regional unconformities beneath the Upper Jurassic Tiaojishan and Lower Cretaceous Zhangjiakou formations (Wong, 1927; Dong et al., 2007, 2015; Zhao et al., 2022). Based on the depositional ages of these formations, the initiations of Phase A and Phase B were constrained to no later than ~165–160 Ma and ~135 Ma, respectively (Zhao et al., 2022). Subsequent studies have identified more tectonic subdivisions (Fig. 2A), reflecting a more complex deformation history (Deng et al., 2007; Dong et al., 2015; Liu et al., 2017, 2019, 2024; Zhu and Xu, 2019; Song et al., 2025). The main characteristics of the Yanshanian orogeny are widespread thrust faults, folds, magmatism and metamorphism in ENC. These fold-and-thrust structures developed during 174–148 Ma, ~170 Ma, indicating the main contractional stage (Fig. 2B) (Song et al., 2025 and references therein). More recently, an earlier tectono-magmatic phase between ~200–175 Ma has been identified and is characterized by magmatism, mineralization, and contractional deformation (Song et al., 2025; Qian and Wang, 2025). In addition to the unconformities below the Tiaojishan Formation and Zhangjiakou Formation, regional unconformities dated to ~200–190 Ma, ~170 Ma, and ~140 Ma are ubiquitous in ENC, indicating episodes of uplift and erosion during the Jurassic to Early Cretaceous (see Geolex: https://chinalex.geolex.org/index.php). For example, in the Yungang and Ningwu-Jingle *syn*-tectonic basins in Shanxi, only the Middle Jurassic and part of the Lower Jurassic strata are preserved (Li et al., 2014; Zhang et al., 2020). These basins developed contemporaneous crustal deformation such as thrusting and folding. The contractional stage (~200 to ~140 Ma) encompasses the most prominent periods of thrusting, folding, and crustal thickening. Although some studies have proposed that localized extensional events may have occurred within this interval (Zhu and Xu, 2019; Qiu et al., 2023; Qian and Wang, 2025), the overall crustal deformation pattern remained dominantly contractional.

Tectonic shortening and magmatic flare-up/underplating could both cause crustal thickening (Lee et al., 2015). But in ENC, tectonic shortening may have played a more important role, given the more widespread contractional deformation structures compared to magmatism during the Jurassic. Circum-craton collisional orogenies during the Triassic and early Jurassic may have caused the initial thickening of the craton margins, but the westward subduction of the Izanagi plate probably played a major role in thickening the crust in ENC (Kusky et al., 2014; Liu et al., 2019; Zhu and Xu, 2019). The dip angle of the subduction slab is a critical factor controlling the deformation of the overriding plate. Generally, a low-angle or flat subduction promotes overriding plate shortening and thickening (Dilek and Ogawa, 2021; Schellart, 2024). For instance, the flat subduction of the Farallon Plate is believed to have caused the Laramide orogeny and regional uplift in North America, and the flat subduction of the Nazca Plate contributed to the formation of the Andes in South America (Liu and Currie, 2016; Manea et al., 2017). There are a number of observations indicating that the Izanagi plate also subducted at a low angle beneath ENC during the Jurassic (Liu et al., 2024). We suggest that the westward low-angle subduction of the Izanagi plate resulted in the widespread crustal thickening in ENC.

The crust remained 60–70 km thick between ~140 and ~110 Ma (Fig. 2). This interval marks a shift from a compressional to tensional regime and is characterized by the coexistence of contractional and extensional structures across ENC. This transitional stage temporally overlapped Phase B of the Yanshanian orogeny, during which contractional structures such as reverse and thrust folds were still actively developing, with some dated to ca. 140–130 Ma and ca. 139–136 Ma (Fig. 2B) (Davis et al., 2001; Song et al., 2025). At the same time, intense magmatism and extensional structures such as half-graben or graben, domes, metamorphic core complex (MCC) exhumation, and extensional basins are also well documented (Fig. 2B) (Lin et al., 2011b; Meng and Lin, 2021; Zhang et al., 2022). For example, the Yunmengshan MCCs in Yanshan were rapidly exhumed between 135–114 Ma and developed a top-to-the SE normal fault during 89–72 Ma. Other MCCs in the Liaodong Peninsula also exhibited similar exhumation timings (Qian and Wang, 2025 and references therein). Early Cretaceous A-type granites are widespread in ENC (Sun and Yang, 2009) and are generally interpreted to have formed in an extensional setting (Loiselle and Wones, 1979). The transition of magma sources from crust-dominated in the Jurassic to mantle-crust hybrid in the Cretaceous may reflect the collapse of the ENC plateau accompanied by the upwelling of mantle materials. While the development of these extensional structures and peak magmatism indicates the onset of extension in ENC, the transition from contraction to extension appears diachronous from east to west. Based on our reconstructed crustal thickness, the initiation of crustal thinning shows a westward younging trend across ENC (Fig. 3). And because of this diachronous transition, significant crustal thinning over the entire ENC area lagged behind the initial extension and occurred between 110 and 80 Ma (Fig. 2).

After 110 Ma, the crustal thickness continued to decrease until about 80 Ma. The thinning process of the crust is less well constrained due to the limited number of zircons (and magmatism) younger than 110 Ma. However, the available data indicate that this thinning process reduced the crust to a thickness close to its modern day. This is also supported by the presence of extensional structures such as detachment faults, normal faults, and MCCs, which developed in Beijing, Hebei, and Liaoning, indicating post-orogenic extension at that time (Davis et al., 2001; Dong et al., 2015; Qian and Wang, 2025). This extensional stage also coincides with tectonic subdivisions identified in previous studies (Fig. 2A) and was likely driven by the rollback of the Izanagi Plate (Liu et al., 2019; Zhu and Xu, 2019).

In summary, based on our crustal thickness reconstruction, the evolution of ENC in the Mesozoic can be divided into three stages: (1) a contractional stage (~200 to ~140 Ma), characterized by thrusting, folding, and crustal thickening; (2) a transitional stage (~140 to ~110 Ma), with coeval contractional and extensional crustal deformation events across ENC; and (3) extensional stage (~110 to ~80 Ma), during which the crust thinned to its modern-day thickness of 30–40 km (Fig. 2C). These interpretations are consistent with other geologic observations compiled in Fig. 2A and discussed above.

5.2. A broad high-elevation plateau in the Mesozoic ENC?

The reconstructed crustal thickness allows us to estimate the paleo-elevation based on the Airy isostasy principle. Our elevation calculation indicates that ENC started from 2–3 km in the early Jurassic and may have reached 4–5 km by approximately 170 Ma. Then in the late Cretaceous, ENC reached its modern-day elevation of <200 m (Fig. 2C). Our results are consistent with independent paleo-elevation estimates from previous studies (Xia et al., 2012; Zhang et al., 2021b). Undoubtedly, our elevation calculations based on Airy isostasy alone are highly simplified, and several other processes may have also caused elevation fluctuations. For example, mantle flow can induce dynamic topography, a quasi-equilibrium state in which normal stresses from pressure variations and vertical flow gradients in the convecting mantle disrupt crustal isostatic balance, leading to elevation changes (Moucha and Forte, 2011; Flament et al., 2013; Turcotte and Schubert, 2014; Lamb et al., 2020). While flow-induced tractions can influence elevation, many studies suggest that they contribute less than 10% to regional

elevation variations (Molnar et al., 2015 and references therein). The influence of the lithospheric mantle on elevation was also ignored in our calculations. This is because the lithospheric mantle plays a secondary role compared to that of the overlying, low-density crust (Tang et al., 2024a). In addition, the complex density structure of the lithospheric mantle also makes it challenging to precisely quantify its impacts on isostatic equilibrium. These simplifications will all lead to uncertainties in our calculated elevations up to 1–2 km. Nevertheless, we suggest that these elevation estimates based on isostasy are sufficient to capture the first-order, multi-kilometer changes in the elevation evolution (Tang et al., 2024a).

Another important question pertains to the spatial extent of the proposed high topographic terrains in ENC during the Mesozoic. Precisely constraining the extent of high-elevation regions in ENC is challenging, but the similar crustal thickening trends seen in all four areas in ENC, including Shanxi, Shandong, Hebei, and Liaoning (Fig. 3), suggest that crustal thickening was widespread across ENC in the Late Jurassic. Widespread crustal thickening is also supported by the ubiquitous contractional structures, including thrust faults and folds, in not only the margins but also the interior of ENC, particularly during the Jurassic (~180–140 Ma) (Wu et al., 2019). We also note that the four areas reached their maximum crustal thicknesses progressively later from east to west, with Liaoning and Shandong undergoing thickening earlier than Hebei and Shanxi. This diachronous thickening trend is consistent with the tempo-spatial distribution of Jurassic magmatic rocks, both of which align with the progressive westward subduction of the Izanagi plate and the landward propagation of upper plate contraction (Wu et al., 2019; Ma and Xu, 2021).

In summary, our findings suggest that much of the ENC may have been uplifted to 4–5 km between 170 and 140 Ma, which points to the existence of a broad high-elevation plateau in ENC during the Mesozoic. This conclusion is consistent with some previous conjectures (Xia et al., 2012; Zhang et al., 2009). This plateau may have extended west to Shanxi Province, separated from Ordos by the Taihang Mountains, as indicated by the synchronous uplift of Taihang Mountains and the ENC plateau since the Jurassic (Wu et al., 2020; Wen et al., 2022). The eastern margin may have reached the Liaoning-Shandong Peninsula and possibly northern Korea, due to similar magmatism and deformation patterns (Dong et al., 2015). The Qinling orogeny lies between North China and South China, forming the southern boundary of the plateau. The Yanshan orogeny, located in the northern part of the North China Craton, may have been the northern margin of the ENC plateau, adjoining the Mongolian Plateau. Recently, a Cretaceous coastal mountain in southern China was reported (Li et al., 2024). This mountain range, together with the ENC plateau, may have formed a vast high-elevation region in East Asia.

5.3. Sedimentary records of plateau erosion

The existence of the ENC plateau is also recorded in sedimentary rocks—detrital zircons in sandstones. The high elevation of the plateau drives a high erosion rate, which in turn is reflected in detrital zircon age distributions. As shown in Fig. 4, the proportion of Mesozoic detrital zircons increases substantially in sandstones deposited from the Early Jurassic to the Late Cretaceous. In addition, there is a notable time lag of 40–50 Myr between the uplift of the plateau and the peak proportion of Mesozoic zircons in sandstones (Fig. 4). This time lag reflects the time required for exhumation and erosion of plutons, as most Mesozoic magmatic rocks in ENC were emplaced as deep-seated plutons (Qiu et al., 2023). Their appearance in sedimentary records is primarily controlled by the erosion rate and the emplacement depth. This allows us to explore the erosion history of the ENC plateau based on our reconstructed topographic evolution path. Critical variables used in the model are listed in Table 1.

We assume that the proportion of Mesozoic zircons is determined by the proportion of eroded Mesozoic magmatic rock, or its erosional flux.

Table 1
List of variables used in the erosion model.

Parameter	Definition	Unit
v	The volumetric rate of total igneous rock formation	km^3/Myr
v_p	The volumetric rate of plutonic rock formation	km^3/Myr
v_v	The volumetric rate of volcanic rock formation	km^3/Myr
v^{ex}_{Meso}	The volumetric addition rate of exposed Mesozoic magmatic rock	km^3/Myr
v^{ex}_{p}	The volumetric addition rate of exposed Mesozoic plutonic rock	km^3/Myr
V_{Meso}	The total relative volumetric addition rate of exposed Mesozoic magmatic rock	km^3
t_{lag}	Time lag	Myr
t_{emp}	Time of magma emplaced	Ma
t_{ex}	Time of pluton exposed at the surface	Ma
D	Intrusive depth	km
E	Erosion rate	km/Myr
S	The eroded area	km^2
H	The crustal thickness	km
H_{Meso}	The thickness of Mesozoic magmatic bodies	km
e_{Meso}	The volumetric erosional flux of Mesozoic magmatic rock	km^3
τ	The erosional response time	Myr
ρ_c	The average density of continental crust (2.74 g/cm^3)	g/cm^3
ρ_m	The average density of mantle (3.24 g/cm^3)	g/cm^3

Here, we define the time lag t_{lag} as the difference in time between magma emplacement (denoted as t_{emp}) and subsequent pluton exposure at the surface (denoted as t_{ex}):

$$t_{lag} = t_{emp}\text{-}t_{ex} \tag{3}$$

t_{lag} can be related to erosion rate (E) and emplacement depth (D) as:

$$t_{lag} = \frac{D}{E} \tag{4}$$

According to Lee et al. (2015), the erosion rate is calculated as a function of elevation related to crustal thickness and erosional response time, τ:

$$E = \frac{1}{\tau} * (1\text{-}\frac{\rho_c}{\rho_m}) * H \tag{5}$$

In addition to elevation, erosion rate is also sensitive to erosional response time, τ, which is influenced by the precipitation rate and substrate erodibility (Simoes et al., 2010). τ tends to be higher in arid climates and lower in moister climates.

The volumetric formation rate of Mesozoic magmatic rocks is linked to the modern magmatic rock distribution from Zhang et al. (2014), which consists of plutonic (v_p) and volcanic rocks (v_v):

$$v_p = v * a/(a+1) \tag{6}$$

$$v_v = v * 1/(a+1) \tag{7}$$

The plutonic/volcanic ratio a is set to 9 (Persikov, 2020). The volumetric addition rate of exposed Mesozoic magmatic rock (v^{ex}_{MZ}) is calculated as the sum of the newly exposed plutonic (v^{ex}_{p}) and volcanic rocks (v_v):

$$v^{ex}_{Meso} = v^{ex}_{p} + v_v \tag{8}$$

The total relative volumetric addition rate of exposed Mesozoic magmatic rocks can be calculated as:

$$dV_{Meso} = (v^{ex}_{Meso}\text{-}e_{Meso})dt \tag{9}$$

The contributions from Mesozoic detritus to downstream sedimentary deposits scales with the volumetric erosional flux of Mesozoic magmatic rock (e_{Meso}), which can be described as:

$$e_{Meso} = S^*E = \frac{V_{Meso}}{H_{Meso}}{}^*E \quad (10)$$

where S represents the eroded area, and H_{Meso} is the thickness of magmatic bodies. For simplicity, we assumed a constant H_{Meso} of 25 km, similar to that of the Lilong batholith in the Gangdese, which developed on thickened crust during Andean-type continental margin orogenesis (Zhang et al., 2014b; Dong et al., 2015).

The volumetric erosional flux of Mesozoic magmatic rock (e_{Meso}) is time-variable and is sensitive to magma emplacement depth (D) and erosional response time (τ). We assume a magma emplacement depth (D) of 10 to 25 km, according to previous studies (Yang et al., 2007; Lin et al., 2011a; Dou et al., 2018). τ is climate-dependent and increases from <5 in moist climates to >25 in arid climates (Simoes et al., 2010). We find that the influence of D on the evolution of e_{Meso} strongly correlates with τ, such that when τ is <5 (moist climate), D has a negligible impact on the timing of maximum e_{Meso}. For a reasonable range of D, a τ of >15 is required to explain the observed time lag between maximum uplift and maximum erosional flux recorded in sedimentary deposits (Fig. 5). This τ corresponds to a precipitation rate of 0.5–1 mm/day, indicative of a relatively arid climate. This finding is consistent with climate models that consider the presence of coastal mountains in East Asia, as well as the $\delta^{13}C$ records in paleosol carbonates, which suggest that the East Asian region experienced arid conditions during the Jurassic period (Zhang et al., 2021b; Jin et al., 2023; Li et al., 2024).

5.4. Connection to the North China Craton destruction

The destruction of the North China Craton is widely accepted to have occurred in the Cretaceous, with peak destruction at ca 125 Ma (Wu et al., 2005, 2019; Zhu et al., 2011, 2012; Yang et al., 2018). Intriguingly, this time period coincides with the onset of collapse of the ENC plateau, pointing to a possible interconnection between the destruction of the North China Craton and the fate of the ENC plateau. The low-angle subduction of the Izanagi plate may have caused extensive crustal contraction and thickening, leading to the rise of the ENC plateau in the Jurassic. In the Cretaceous, the subduction angle of the Izanagi plate steepened, and as a consequence, trench pull-back may have induced deviatoric tensional normal stresses, while mantle return flow, interacting with the overriding plate, which increased basal shear drag. These interactions may have resulted in the widespread lithospheric extension (Wang et al., 2016; Schellart, 2024), which in turn triggered the collapse of the plateau, intense magmatism, as well as massive destruction of the cratonic mantle beneath ENC (Kusky et al., 2014). Hence, both the collapse of the ENC plateau and destruction of the underlying mantle keel were the consequences of the rollback of the subducting Izanagi plate. Additionally, the formation of dense eclogitic lower crust during the development of the ENC plateau may have further increased the gravitational instability of the ENC lithosphere, ultimately contributing to its destruction through delamination, as shown in Fig. 6 (Deng et al., 2007; Wang et al., 2018b, 2022b; Wu et al., 2019; Chen et al., 2023a; Liu et al., 2023).

The spatial and temporal overlap between the North China Craton destruction and ENC plateau collapse highlights the pivotal role of Izanagi plate subduction in shaping the tectonics and mantle dynamics across East Asia during the Mesozoic. This influence may have extended further south, driving the formation of extensive mountain ranges in southern China during the Cretaceous (Li et al., 2024). The emergence of such a vast high-elevation region in East Asia likely played a crucial role in modulating moisture transport routes and precipitation patterns. Recent studies suggest that the presence of extensive high topographies could interrupt moisture transport from the Tethys and Pacific, leading to reduced rainfall in inland areas and the expansion of arid zones (Li et al., 2024; Wang et al., 2024; Zhang et al., 2021a). Our study provides constraints on the rise and fall of the ENC plateau. Future modeling efforts taking these new constraints into account may shed new light on the coupling between tectonics and climate in East Asia during the Mesozoic.

6. Conclusions

We carried out extensive sampling of detrital zircons from modern river sands and ancient sandstones to constrain the evolution of crustal thickness in ENC. The Eu anomalies of these detrital zircons, combined with observations of crustal deformation patterns and magmatism, suggest that the crust of ENC thickened to approximately 60–70 km in the Early Jurassic and then thinned to ~35 km in the Late Cretaceous. Crustal thickening in the Jurassic appears to have been prevalent in the entire ENC. These results are consistent with the presence of a vast plateau, with elevations comparable to modern Tibet or the Andes, in ENC during the Middle Jurassic to Early Cretaceous.

The rise and fall of the ENC plateau are also recorded in the U-Pb age

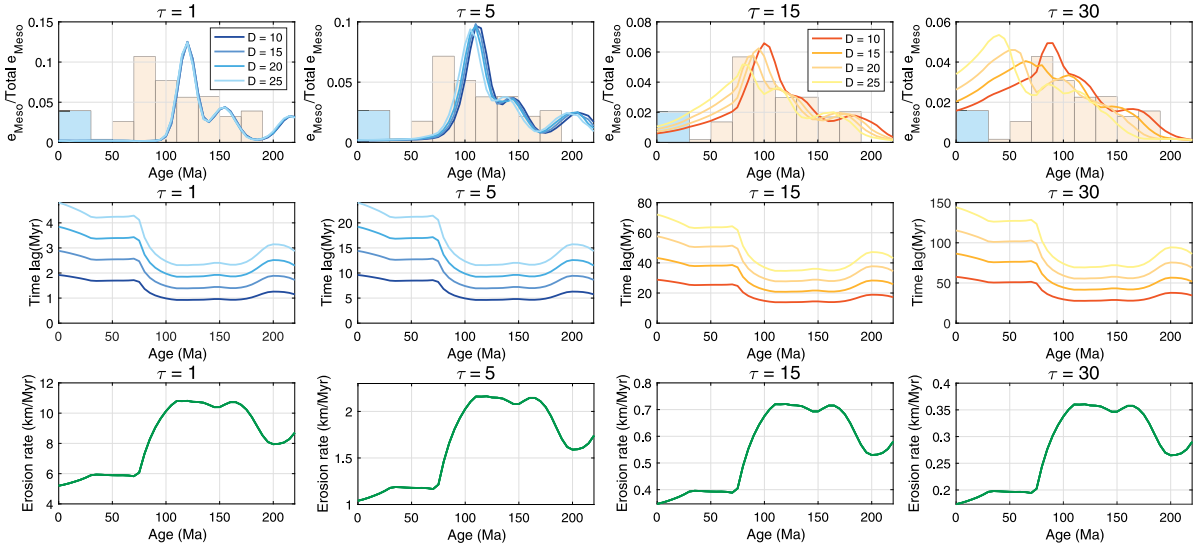


Fig. 5. Uplift and erosion model with different τ and D. (A) Observed Mesozoic zircon proportion in sandstones (histogram) from Fig. 4 and modeled Mesozoic zircon proportion (curve). (B) Time lag. (C) Erosion rate. We normalized e_{Meso} by dividing each value by its total volumetric erosional flux of Mesozoic magmatic rock (e^{Total}_{Meso}) to render it dimensionless and focus solely on the relative trend.

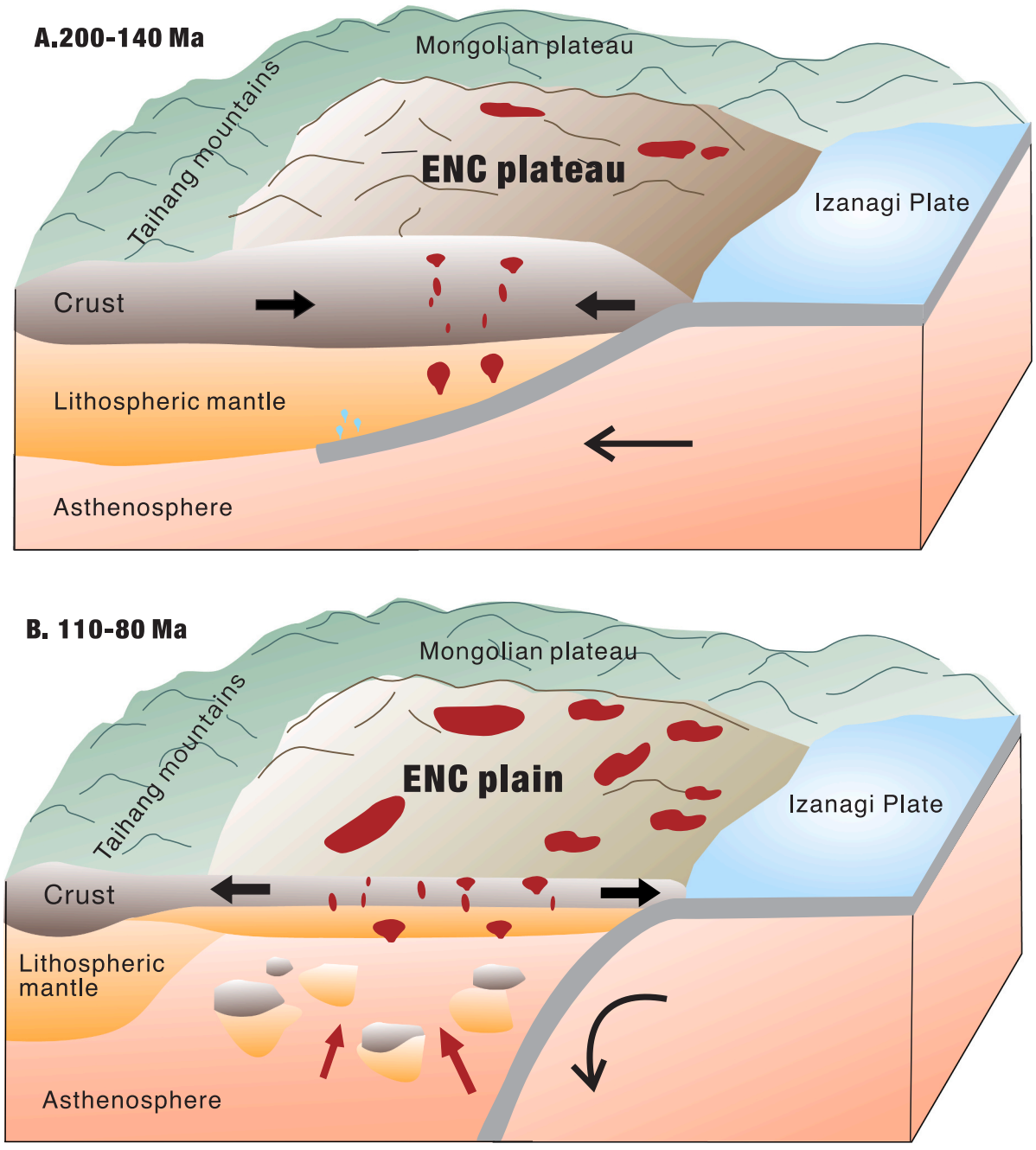


Fig. 6. Cartoon showing the formation (A) and collapse (B) of ENC plateau in the Mesozoic. Cartoon is not to scale.

distributions of detrital zircons in sandstones deposited in different time periods since the early Jurassic. Based on our modeling, the erosion of the ENC plateau likely took place in a largely arid climate, consistent with other geologic observations.

The rise of the ENC plateau was likely a consequence of crustal compression caused primarily by the flat subduction of the Izanagi plate. The collapse of the ENC plateau was likely triggered by the rollback of the Izanagi plate and resulted in lithospheric thinning and mantle upwelling, accompanied by extensive crustal- and mantle-derived magmatism. The interplay of these processes may have culminated in the destruction of the North China Craton.

Data availability

Supplementary Material 2 with 3 datasets is available through Mendeley Data at https://doi.org/10.17632/kkz4dcd944.1.

CRediT authorship contribution statement

Ziyi Guo: Methodology, Data curation, Visualization, Formal analysis, Writing – original draft, Investigation, Conceptualization. **Ming Tang:** Methodology, Conceptualization, Writing – review & editing, Funding acquisition, Investigation. **Hehe Jiang:** Writing – review & editing, Investigation. **Xuyang Zheng:** Investigation, Writing – review & editing.

Declaration of competing interest

The authors declare that they have no known competing financial interests or personal relationships that could have appeared to influence

the work reported in this paper.

Acknowledgements

We thank the Editor Hailiang Dong and the Associate Editor Fangzhen Teng for their efficient editorial handling. We appreciate the constructive comments of professor Timothy M. Kusky and two anonymous reviewers, which greatly improved the presentation of this work. We also thank our colleagues Hao Chen, Xuanyu Liu, Jiazhen Wang, Zi Ye and Junteng Lyu for their assistance during sample collection and discussions. This work was financially supported by National Natural Science Foundation of China (grants 42125302, 92355301, and 41888101). M. T. is grateful for the support from the New Cornerstone Science Foundation through the XPLORER PRIZE.

Appendix A. Supplementary material

Supplementary Material 1 contains the supplementary figures and the detail information of the sample sites. Supplementary Material 2 contains Dataset 1, which includes all detrital zircon U-Pb dating and trace element compositions analyzed in this study, Dataset 2, which compiles detrital zircon age data of sandstones from previous studies, and Dataset 3, which compiles whole-rock data for calculating crustal thickness. Supplementary material to this article can be found online at https://doi.org/10.1016/j.gca.2025.06.019.

References

Airy, G.B., 1855. On the computation of the effect of the attraction of mountain-masses, as disturbing the apparent astronomical latitude of stations in geodetic surveys. Philos. Trans. R. Soc. Lond. 145, 101–104.

Chen, H., Tang, M., Song, S.-G., 2023a. Catastrophic craton destruction via wholesale lithosphere delamination. Geology 51, 460–464.

Chen, L., 2009. Lithospheric structure variations between the eastern and central North China Craton from S- and P-receiver function migration. Phys. Earth Planet. In. 173, 216–227.

Chen, Z., Zhou, J.-B., Li, G.-Y., Wilde, S.A., 2023b. The nature and spatial–temporal evolution of suture zones in Northeast China. Earth Sci. Rev. 241, 104437.

Davis, G.A., Zheng, Y., Wang, C., Darby, B.J., Zhang, C.H., Gehrels, G., 2001. Mesozoic tectonic evolution of the Yanshan fold and thrust belt, with emphasis on Hebei and Liaoning provinces, northern China. From Continental Assembly to Intracontinental Deformation Geological Society of America, In Paleozoic and Mesozoic Tectonic Evolution of Central and Eastern Asia, pp. 171–197.

Deng, J., Su, S., Niu, Y., Liu, C., Zhao, G., Zhao, X., Zhou, S., Wu, Z., 2007. A possible model for the lithospheric thinning of North China Craton: evidence from the Yanshanian (Jura-cretaceous) magmatism and tectonism. Lithos 96, 22–35.

Dilek, Y., Ogawa, Y., 2021. Subduction zone processes and crustal growth mechanisms at Pacific Rim convergent margins: modern and ancient analogues. Geol. Mag. 158, 1–12.

Diwu, C., Sun, Y., Si, B.W., Yan, M.J., 2024. Archean continental crustal growth and reworking of the North China Craton: Constraints from zircon U Pb age and Hf isotopic composition. Earth Sci. Rev. 248, 104624.

Dong, S.W., Zhang, Y.Q., Zhang, F.Q., Cui, J., Chen, X.H., Zhang, S.H., Miao, L.C., Li, J. H., Shi, W., Li, Z.H., Huang, S.Q., Li, H.L., 2015. Late Jurassic–Early cretaceous continental convergence and intracontinental orogenesis in East Asia: a synthesis of the Yanshan Revolution. J. Asian Earth Sci. 114, 750–770.

Dong, S., Zhang, Y., Long, C., Yang, Z., Ji, Q., Wang, T., Hu, J., Chen, X., 2007. Jurassic tectonic revoution in China and new. Acta Geol. Sin. 81, 1449–1461 in Chinese with English abstract.

Dong, Y., Zhang, G., Neubauer, F., Liu, X., Genser, J., Hauzenberger, C., 2011. Tectonic evolution of the Qinling orogen, China: Review and synthesis. J. Asian Earth Sci. 41, 213–237.

Dou, J.-Z., Zhang, H.-F., Tong, Y., Wang, F., Chen, F.-K., Li, S.-R., 2018. Application of geothermo-barometers to Mesozoic granitoids in the Jiaodong Peninsula, eastern China: Criteria for selecting methods of pressure estimation and implications for crustal exhumation. J. Asian Earth Sci. 160, 271–286.

Flament, N., Gurnis, M., Müller, R.D., 2013. A review of observations and models of dynamic topography. Lithosphere 5, 189–210.

Huang, C., Wang, H., Yang, J., Ramezani, J., Yang, C., Zhang, S., Yang, Y., Xia, X., Feng, L., Lin, J., Wang, T., Ma, Q., He, H., Xie, L., Wu, S., 2019. SA01 – a Proposed Zircon Reference Material for Microbeam U-Pb Age and Hf-O Isotopic Determination. Geostandard Geoanalytic Res 44, 103–123.

Isozaki, Y., Aoki, K., Nakama, T., Yanai, S., 2010. New insight into a subduction-related orogen: a reappraisal of the geotectonic framework and evolution of the Japanese Islands. Gondw. Res. 18, 82–105.

Jin, T., Zhang, L., Huntington, K.W., Wen, Y., Schauer, A.J., Gu, X., Wang, C., 2023. Differential paleoelevation changes in North China during the late Mesozoic: evidence from stable isotopes and clumped isotopes. Global Planet. Change 230, 104275.

Kusky, T.M., Li, J., 2003. Paleoproterozoic tectonic evolution of the North China Craton. J. Asian Earth Sci. 22, 383–397.

Kusky, T.M., Polat, A., Windley, B.F., Burke, K.C., Dewey, J.F., Kidd, W.S.F., Maruyama, S., Wang, J.P., Deng, H., Wang, Z.S., Wang, C., Fu, D., Li, X.W., Peng, H. T., 2016. Insights into the tectonic evolution of the North China Craton through comparative tectonic analysis: a record of outward growth of Precambrian continents. Earth Sci. Rev. 162, 387–432.

Kusky, T.M., Windley, B.F., Wang, L., Wang, Z., Li, X., Zhu, P., 2014. Flat slab subduction, trench suction, and craton destruction: Comparison of the North China, Wyoming, and Brazilian cratons. Tectonophysics 630, 208–221.

Kusky, T.M., Windley, B.F., Zhai, M.G., 2007a. Lithospheric thinning in eastern Asia; constraints, evolution, and tests of models. In Mesozoic Sub-Continental Lithospheric Thinning under Eastern Asia Geological Society of London Special Publication. 331–343.

Kusky, T.M., Windley, B.F., Zhai, M.G., 2007b. Tectonic evolution of the North China Block: from orogen to craton to orogen. In Mesozoic Sub-Continental Lithospheric Thinning under Eastern Asia Geological Society of London Special Publication. 1–34.

Lamb, S., Moore, J.D.P., Perez-Gussinye, M., Stern, T., 2020. Global whole Lithosphere Isostasy: Implications for Surface Elevations, Structure, Strength, and Densities of the Continental Lithosphere. Geochem. Geophys. Geosyst. 21, e2020GC009150.

Lee, C.-T.-A., Thurner, S., Paterson, S., Cao, W., 2015. The rise and fall of continental arcs: Interplays between magmatism, uplift, weathering, and climate. Earth Planet. Sci. Lett. 425, 105–119.

Li, J.H., Dong, S.W., Zhao, G.C., Cawood, P.A., Johnston, S.T., Zhang, J., Xin, Y.J., Wang, J.M., 2024. Cretaceous coastal mountain building and potential impacts on climate change in East Asia. Sci. Adv. 10, eads0587.

Li, S., Zhao, G., Dai, L., Liu, X., Zhou, L., Santosh, M., Suo, Y., 2012. Mesozoic basins in eastern China and their bearing on the deconstruction of the North China Craton. J. Asian Earth Sci. 47, 64–79.

Li, Z., Dong, S., Qu, H., 2014. Timing of the initiation of the Jurassic Yanshan movement on the North China Craton: evidence from sedimentary cycles, heavy minerals, geochemistry, and zircon U–Pb geochronology. Int. Geol. Rev. 56, 288–312.

Li, Z.-X., Liu, Y., Ernst, R., 2023. A dynamic 2000—540 Ma Earth history: from cratonic amalgamation to the age of supercontinent cycle. Earth Sci. Rev. 238, 104336.

Liang Y., Guo W., Ma Y. and Zhao E. (2020) Geochemical Evidence for Thickening and Thinning of Lower Crust beneath the Jiaodong Peninsula: Implications for Late Mesozoic Destruction of the Eastern North China Craton ed. S. Carretier. *Lithosphere* **2020**, 8831664.

Lin, W., Monié, P., Faure, M., Schärer, U., Shi, Y., Breton, N.L., Wang, Q., 2011a. Cooling paths of the NE China crust during the Mesozoic extensional tectonics: example from the south-Liaodong peninsula metamorphic core complex. J. Asian Earth Sci. 42, 1048–1065.

Lin, W., Wang, Q.C., Wang, J., Wang, F., Chu, Y., Chen, K., 2011b. Late Mesozoic extensional tectonics of the Liaodong Peninsula massif: Response of crust to continental lithosphere destruction of the North China Craton. Sci. China Earth Sci. 54, 843–857.

Liu, J.G., Cai, R.H., Pearson, D.G., Scott, J.M., 2019. Thinning and destruction of the lithospheric mantle root beneath the North China Craton: a review. Earth Sci. Rev. 196, 102873.

Liu, S.B., Currie, C.A., 2016. Farallon plate dynamics prior to the Laramide orogeny: Numerical models of flat subduction. Tectonophysics 666, 33–47.

Liu, S.F., Zhang, B., Ma, P.F., Williams, S., Lin, C.F., Wan, N., Ran, C.L., Gurnis, M., 2024. Craton deformation from flat-slab subduction and rollback. Nat. Geosci. 17, 936–943.

Liu, S., Gurnis, M., Ma, P., Zhang, B., 2017. Reconstruction of northeast asian deformation integrated with western Pacific plate subduction since 200 Ma. Earth Sci. Rev. 175, 114–142.

Liu, Y., Wei, J.H., Zhang, D.H., Liu, X., Yan, Z.Q., Tan, J., 2023. Mesozoic crustal reworking at different depths in the North China Craton: Insight from the coexisting Early cretaceous high and low Sr/Y granitoids. Lithos 462–463, 107402.

Loiselle, M.C., Wones, D.R., 1979. Characteristics and origin of anorogenic granites. Geol. Soc. Am. 11, 468.

Ma, Q., Xu, Y.-G., 2021. Magmatic perspective on subduction of Paleo-Pacific plate and initiation of big mantle wedge in East Asia. Earth Sci. Rev. 213, 103473.

Manea, V.C., Manea, M., Ferrari, L., Orozco-Esquivel, T., Valenzuela, R.W., Husker, A., Kostoglodov, V., 2017. A review of the geodynamic evolution of flat slab subduction in Mexico, Peru, and Chile. Tectonophysics 695, 27–52.

Maruyama, S., Isozaki, Y., Kimura, G., Terabayashi, M., 1997. Paleogeographic maps of the Japanese Islands: Plate tectonic synthesis from 750 Ma to the present. Isl. Arc 6, 121–142.

Meng, L., Lin, W., 2021. Episodic Crustal Extension and Contraction Characterizing the late Mesozoic Tectonics of East China: evidence from the Jiaodong Peninsula, East China. Tectonics 40, e2020TC006318.

Molnar, P., England, P.C., Jones, C.H., 2015. Mantle dynamics, isostasy, and the support of high terrain. JGR Solid Earth 120, 1932–1957.

Moucha, R., Forte, A.M., 2011. Changes in african topography driven by mantle convection. Nature Geosci 4, 707–712.

Ouyang, H., Mao, J., Zhou, Z., Su, H., 2015. Late Mesozoic metallogeny and intracontinental magmatism, southern Great Xing'an Range, northeastern China. Gondw. Res. 27, 1153–1172.

Pan, Y., Sha, J., Zhou, Z., Fürsich, F.T., 2013. The Jehol Biota: Definition and distribution of exceptionally preserved relicts of a continental Early cretaceous ecosystem. Cretac. Res. 44, 30–38.

Persikov, E.S., 2020. Distribution of Felsic-Mafic Intrusive and Extrusive Rocks in the Earth's Crust: Correlation with Magma Viscosity Regularities. Russ. Geol. Geophys. 61, 592–599.
Qian, Q., Wang, Y., 2025. Episodic tectonism, metamorphism, magmatism, mineralization and mass mortality in eastern China (and adjacent regions) during the Yanshanian movement: Consequences of major global plate reorganizations during the main episodes of Pangea breakup? Earth Sci. Rev. 265, 105107.
Qin, J.F., Lai, S.C., Grapes, R., Diwu, C.R., Ju, Y.J., Li, Y.F., 2009. Geochemical evidence for origin of magma mixing for the Triassic monzonitic granite and its enclaves at Mishuling in the Qinling orogen (central China). Lithos 112, 259–276.
Qiu, H., Lin, W., Chen, Y., Faure, M., 2023. Jurassic–Early cretaceous tectonic evolution of the North China Craton and Yanshanian intracontinental orogeny in East Asia: New insights from a general review of stratigraphy, structures, and magmatism. Earth Sci. Rev. 237, 104320.
Roberts, N.M.W., Spencer, C.J., Puetz, S., Keller, C.B., Tapster, S., 2024. Regional trends and petrologic factors inhibit global interpretations of zircon trace element compositions. Geosci. Front. 15, 101852.
Schellart, W.P., 2024. Subduction dynamics and overriding plate deformation. Earth Sci. Rev. 253, 104755.
Simoes, M., Braun, J., Bonnet, S., 2010. Continental-scale erosion and transport laws: a new approach to quantitatively investigate macroscale landscapes and associated sediment fluxes over the geological past. Geochem. Geophys. Geosyst. 11, 2010GC003121.
Song, Z., Liang, C., Neubauer, F., Liu, Y., Zheng, C., Lin, B., Xu, X., 2025. The Yanshanian Movement in Western Liaoning, northeastern North China Craton. Earth Sci. Rev. 260, 104989.
Sorokin, A.A., Zaika, V.A., Kovach, V.P., Kotov, A.B., Xu, W.L., Yang, H., 2020. Timing of closure of the eastern Mongol–Okhotsk Ocean: Constraints from U–Pb and Hf isotopic data of detrital zircons from metasediments along the Dzhagdy Transect. Gondw. Res. 81, 58–78.
Sun, J., Yang, J., 2009. Early cretaceous A-type granites in the eastern North China Block with relation to destruction of the craton. Earth Sci. 34, 137–147.
Sun, W., Li, S., Chen, Y., Li, Y., 2002. Timing of Synorogenic Granitoids in the South Qinling, Central China: Constraints on the Evolution of the Qinling-Dabie Orogenic Belt. J. Geol. 110, 457–468.
Tang, M., Chen, H., Lee, C.-T.-A., Cao, W., 2024a. Subaerial crust emergence hindered by phase-driven lower crust densification on early Earth. Sci. Adv. 10, eadq1952.
Tang, M., Guo, Z., Cao, W., Chu, X., 2024b. Revisiting zircon Eu anomaly as a proxy for crustal thickness: a case study of the Sierra Nevada Batholith. Earth Planet. Sci. Lett. 643, 118897.
Tang, M., Ji, W.-Q., Chu, X., Wu, A., Chen, C., 2021. Reconstructing crustal thickness evolution from europium anomalies in detrital zircons. Geology 49, 76–80.
Turcotte, D.L., Schubert, G., 2014. *Geodynamics*, 3rd ed. Cambridge University Press, Cambridge.
Van Der Voo, R., Van Hinsbergen, D.J.J., Domeier, M., Spakman, W., Torsvik, T.H., 2015. Latest Jurassic–earliest cretaceous closure of the Mongol-Okhotsk Ocean: a paleomagnetic and seismological-tomographic analysis. Geol. Soc. Am. Spec. Paper 513, 589–606.
Wan, B., Li, S., Xiao, W., Windley, B.F., 2018. Where and when did the Paleo-asian ocean form? Precambr. Res. 317, 241–252.
Wang, T., Tong, Y., Xiao, W., Guo, L., Windley, B.F., Donskaya, T., Li, S., Tserendash, N., Zhang, J., 2022a. Rollback, scissor-like closure of the Mongol-Okhotsk Ocean and formation of an orocline: magmatic migration based on a large archive of age data. Natl. Sci. Rev. 9, nwab210.
Wang, T., Wang, X., Tian, W., Zhang, C., Li, W.P., Li, S., 2009. North Qinling Paleozoic granite associations and their variation in space and time: Implications for orogenic processes in the orogens of central China. Sci. China Ser. D-Earth Sci. 52, 1359–1384.
Wang, W., Chu, X., Zhang, J., Cui, Y., Chen, X., Wang, Y., Su, S., 2024. The climatic pattern of East Asia shifted in response to cratonic thinning in the Early cretaceous. Commun. Earth Environ. 5, 728.
Wang, Y.F., Hu, Z.D., Zheng, Y.D., 1990. The Charactertstics and K-Ar Age of Clay Minerals in the Fault Gouges in the Yunmeng Mountains, Betlmg, China. Phys. Chem. Earth 17, 25–32.
Wang, Y., Zhou, L.Y., Liu, S.F., Li, J.Y., Yang, T.N., 2018a. Post-cratonization deformation processes and tectonic evolution of the North China Craton. Earth Sci. Rev. 177, 320–365.
Wang, Z., Capitanio, F.A., Wang, Z., Kusky, T.M., 2022b. Accretion of the cratonic mantle lithosphere via massive regional relamination. Proc. Natl. Acad. Sci. U.S.A. 119, e2201226119.
Wang, Z., Kusky, T.M., Capitanio, F.A., 2016. Lithosphere thinning induced by slab penetration into a hydrous mantle transition zone. Geophys. Res. Lett. 43.
Wang, Z., Kusky, T.M., Capitanio, F.A., 2018b. On the Role of lower Crust and Midlithosphere Discontinuity for Cratonic Lithosphere Delamination and Recycling. Geophys. Res. Lett. 45, 7425–7433.
Wei, Z., Chu, R., Chen, L., 2015. Regional differences in crustal structure of the North China Craton from receiver functions. Sci. China Earth Sci. 58, 2200–2210.
Wen, Y., Zhang, L., Li, Y., Huntington, K.W., Jin, T., Schauer, A.J., Wang, C., 2022. Late Mesozoic elevation history of the north Taihang Mountains. Constraints from clumped isotope geochemistry. GSA Bulletin, China.
Wong, W.H., 1927. Crustal Movements and Igneous Activities in Eastern China since Mesozoic Time.[1]. Bull. Geol. Soc. China 6, 9–37.
Wu, F., Lin, J., Wilde, S., Zhang, X., Yang, J., 2005. Nature and significance of the Early cretaceous giant igneous event in eastern China. Earth Planet. Sci. Lett. 233, 103–119.
Wu, F., Yang, J., Lo, C., Wilde, S.A., Sun, D., Jahn, B., 2007. The Heilongjiang Group: a Jurassic accretionary complex in the Jiamusi Massif at the western Pacific margin of northeastern China. Isl. Arc 16, 156–172.
Wu, F.-Y., Yang, J.-H., Xu, Y.-G., Wilde, S.A., Walker, R.J., 2019. Destruction of the North China Craton in the Mesozoic. Annu. Rev. Earth Planet. Sci. 47, 173–195.
Wu, L., Wang, F., Yang, J., Wang, Y., Zhang, W., Yang, L., Shi, W., 2020. Meso-Cenozoic uplift of the Taihang Mountains, North China: evidence from zircon and apatite thermochronology. Geol. Mag. 157, 1097–1111.
Wu, Y.-B., Zheng, Y.-F., 2013. Tectonic evolution of a composite collision orogen: an overview on the Qinling–Tongbai–Hong'an–Dabie–Sulu orogenic belt in central China. Gondw. Res. 23, 1402–1428.
Xia, B., Thybo, H., Artemieva, I.M., 2020. Lithosphere Mantle Density of the North China Craton. *JGR*. Solid Earth 125, e2020JB020296.
Xia, B., Thybo, H., Artemieva, I.M., 2017. Seismic crustal structure of the North China Craton and surrounding area: Synthesis and analysis. JGR Solid Earth 122, 5181–5207.
Xia, G.-Q., Yi, H.-S., Zhao, X.-X., Gong, D.-X., Ji, C.-J., 2012. A late Mesozoic high plateau in eastern China: evidence from basalt vesicular paleoaltimetry. Chin. Sci. Bull. 57, 2767–2777.
Xiao, W., Windley, B.F., Sun, S., Li, J., Huang, B., Han, C., Yuan, C., Sun, M., Chen, H., 2015. A Tale of Amalgamation of three Permo-Triassic Collage Systems in Central Asia: Oroclines, Sutures, and Terminal Accretion. Annu. Rev. Earth Planet. Sci. 43, 477–507.
Xu, B., Charvet, J., Chen, Y., Zhao, P., Shi, G.Z., 2013. Middle Paleozoic convergent orogenic belts in western Inner Mongolia (China): framework, kinematics, geochronology and implications for tectonic evolution of the Central Asian Orogenic Belt. Gondw. Res. 23, 1342–1364.
Yakymchuk, C., Holder, R.M., Kendrick, J., Moyen, J.-F., 2023. Europium anomalies in zircon: a signal of crustal depth? Earth Planet. Sci. Lett. 622, 118405.
Yang, F., Santosh, M., Tang, L., 2018. Extensive crustal melting during craton destruction: evidence from the Mesozoic magmatic suite of Junan, eastern North China Craton. J. Asian Earth Sci. 157, 119–140.
Yang, J., Wu, F., Liu, X., Xie, L., Yang, Y., 2007. Petrogenesis and geological significance of the Jurassic Xiaoheishan pluton in the Liaodong Peninsula, East China: In-situ zircon U-Pb dating and Hf isotopic analysis. Bull. Mineral. Petrol. Geochem. 26, 29–43.
Yang, J., Wu, F., Shao, J., Wilde, S., Xie, L., Liu, X., 2006. Constraints on the timing of uplift of the Yanshan Fold and Thrust Belt, North China. Earth Planet. Sci. Lett. 246, 336–352.
Zeng, J., Lin, W., Qiu, H., Wei, W., Meng, L., Chu, Y., Ren, Z., Wang, Y., Feng, Z., 2022. When did the large-scale extensional tectonics begin in North China Craton? Tectonophysics 840, 229563.
Zhang L., Yin Y. and Wang C. (2021b) High-Altitude and Cold Habitat for the Early Cretaceous Feathered Dinosaurs at Sihetun, Western Liaoning, China. *Geophysical Research Letters* **48**, e2021GL094370.
Zhang, Q., Jiao, S.-T., 2020. Adakite comes from a high-pressure background: a scientific, reliable, predictable scientific discovery. Acta Petrol. Sin. 36, 1675–1683 in Chinese with English abstract.
Zhang, Q., Wang, Y., Jin, W.-J., Li, C.-D., 2009. Eastern China Plateau during the late Mesozoic: evidence, problems and implication. Geol. Bull. China 27, 3466–3492 in Chinese with English abstract.
Zhang, S.-H., Zhao, Y., Davis, G.A., Ye, H., Wu, F., 2014a. Temporal and spatial variations of Mesozoic magmatism and deformation in the North China Craton: Implications for lithospheric thinning and decratonization. Earth Sci. Rev. 131, 49–87.
Zhang, J., Liu, Y., Flögel, S., Zhang, T., Wang, C., Fang, X., 2021a. Altitude of the East Asian Coastal Mountains and their Influence on asian climate during Early late cretaceous. JGR Atmospheres 126, e2020JD034413.
Zhang, Y., Qiu, E., Dong, S., Li, J., Shi, W., 2022. Late Mesozoic intracontinental deformation and magmatism in North and NE China in response to multi-plate convergence in NE Asia: an overview and new view. Tectonophysics 835, 229377.
Zhang, Y., Shi, W., Dong, S., Wang, T., Yang, Q., 2020. Jurassic intracontinental deformation of the central North China Plate: Insights from syn-tectonic sedimentation, structural geology, and UPb geochronology of the Yungang Basin. North China. Tectonophysics 778, 228371.
Zhang, Z., Dong, X., Xiang, H., He, Z., Liou, J.G., 2014b. Metagabbros of the Gangdese arc root, south Tibet: Implications for the growth of continental crust. Geochim. Cosmochim. Acta 143, 268–284.
Zhang, Z.-J., Kusky, T., Gao, M., Cheng, Q.-M., 2023. Spatio-temporal analysis of big data sets of detrital zircon U-Pb geochronology and Hf isotope data: Tests of tectonic models for the Precambrian evolution of the North China Craton. Earth Sci. Rev. 239, 104372.
Zhao, G., Cawood, P.A., Wilde, S.A., Sun, M., Lu, L., 2000. Metamorphism of basement rocks in the Central Zone of the North China Craton: implications for Paleoproterozoic tectonic evolution. Precambr. Res. 103, 55–88.
Zhao, G., Wilde, S.A., Cawood, P.A., Sun, M., 2001. Archean blocks and their boundaries in the North China Craton: lithological, geochemical, structural and P–T path constraints and tectonic evolution. Precambr. Res. 107, 45–73.
Zhao, G., Zhai, M., 2013. Lithotectonic elements of Precambrian basement in the North China Craton: Review and tectonic implications. Gondw. Res. 23, 1207–1240.
Zhao, L., Tang, H., Mitchell, R.N., Li, Q.L., Zhou, X.W., Zhai, M.G., 2023. The joining of North and South China during the Permian: Coherent Metamorphic evidence from East Asia Orogenesis. Tectonics 42, e2023TC007916.
Zhao, P., Jia, Z.H., Xu, B., Xu, Y., Sukhbaatar, T., Appel, E., Chen, Y., 2024. Late Triassic initial closure of the Mongol-Okhotsk Ocean in the western segment: Constraints

from sedimentological, detrital zircon ages and paleomagnetic evidence. Gondw. Res. 125, 110–129.
Zhao, Y., Gao, H.L., Zhang, S.H., Liu, J., 2022. A brief century review of the "Yanshan Movement" and its founder. Acta Geol. Sin. 96, 1510–1523 in Chinese with English abstract.
Zhou, J.-B., Li, L., 2017. The Mesozoic accretionary complex in Northeast China: evidence for the accretion history of Paleo-Pacific subduction. J. Asian Earth Sci. 145, 91–100.
Zhou, Z., Meng, Q., Zhu, R.X., Wang, M., 2021. Spatiotemporal evolution of the Jehol Biota: responses to the North China craton destruction in the Early cretaceous. Proc. Natl. Acad. Sci. U.S.A. 118, e2107859118.
Zhu, G., Chen, Y., Jiang, D.Z., Lin, S., 2015. Rapid change from compression to extension in the North China Craton during the Early cretaceous: evidence from the Yunmengshan metamorphic core complex. Tectonophysics 656, 91–110.
Zhu, R., Chen, L., Wu, F., Liu, J., 2011. Timing, scale and mechanism of the destruction of the North China Craton. Sci. China Earth Sci. 54, 789–797.
Zhu, R.X., Xu, Y.G., 2019. The subduction of the west Pacific plate and the destruction of the North China Craton. Sci. China Earth Sci. 62, 1340–1350.
Zhu, R.X., Zhao, G.C., Xiao, W.J., Chen, L., Tang, Y.J., 2021. Origin, Accretion, and Reworking of Continents. Rev. Geophys. 59, e2019RG000689.
Zhu, R.-X., Yang, J.-H., Wu, F.-Y., 2012. Timing of destruction of the North China Craton. Lithos 149, 51–60.